

Dynamics of doublon-holon pairs in Hubbard two-leg ladders

Luis G. G. V. Dias da Silva,¹ G. Alvarez,² and E. Dagotto³

¹*Instituto de Física, Universidade de São Paulo, C.P. 66318, São Paulo, SP, Brazil, 05315-970.*

²*Computer Science & Mathematics Division and Center for Nanophase Materials Sciences, Oak Ridge National Laboratory, Oak Ridge, TN 37831, USA*

³*Department of Physics and Astronomy, University of Tennessee, Knoxville, Tennessee 37996, USA, and Materials Science and Technology Division, Oak Ridge National Laboratory, Oak Ridge, Tennessee 37831, USA*

(Dated: June 21, 2021)

The dynamics of holon-doublon pairs is studied in Hubbard two-leg ladders using the time-dependent Density Matrix Renormalization Group method. We find that the geometry of the two-leg ladder, that is qualitatively different from a one-dimensional chain due to the presence of a spin-gap, strongly affects the propagation of a doublon-holon pair. Two distinct regimes are identified. For weak inter-leg coupling, the results are qualitatively similar to the case of the propagation previously reported in Hubbard chains, with only a renormalization of parameters. More interesting is the case of strong inter-leg coupling where substantial differences arise, particularly regarding the double occupancy and properties of the excitations such as the doublon speed. Our results suggest a connection between the presence of a spin gap and qualitative changes in the doublon speed, indicating a weak coupling between the doublon and the magnetic excitations.

PACS numbers: 71.10.Fd, 71.10.Li, 71.35.-y

I. INTRODUCTION

Quasi-one dimensional correlated quantum systems have received considerable attention from the Condensed Matter community because they display exotic properties that arise from the dimensional confinement of electrons. A famous example are the quantum spin systems with the geometry of “ladders”, namely infinitely long one-dimensional “legs” that are coupled along “rungs” via tight binding hopping terms with strengths comparable or larger than those along the legs.¹ Previous research has shown that ladders with an odd number of legs behave similarly as truly one-dimensional systems in the sense that spin-spin correlations decay with distance following power laws. However, for even number of legs (two in particular) the decay is exponential due to the presence of a so-called spin gap.²⁻⁵ The existence of this spin gap has been confirmed experimentally in materials such as the copper oxide SrCu_2O_3 . For the case of two-leg ladders, the spin gap is caused by the dominance of spin singlet configurations along the rungs, which have a spin gap between singlet and triplet states. The existence of a ground state dominated by spin singlet arrangements resembling resonant valence bond states, and other properties such as the prediction of superconductivity upon doping, have established interesting analogies between two-leg ladders and the two-dimensional high temperature superconductors based on CuO_2 layers.⁶ Two-leg ladders can also be found in the context of organic compounds such as BPCB $((\text{C}_5\text{H}_{12}\text{N})_2\text{CuBr}_4)$,⁷ showing that the importance of two-leg ladders is not only restricted by its similarity with the high- T_c cuprates but it is broader, covering several families of materials.

The studies of two-leg ladders are not restricted to spin systems, but considerable work has been devoted to the

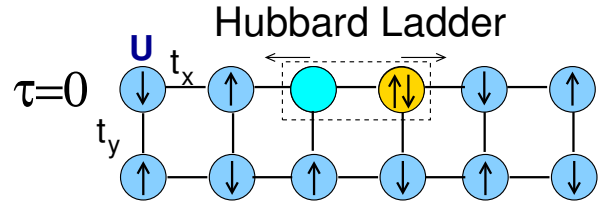


FIG. 1: (Color online) Creation of a doublon-holon pair in a two-leg Hubbard ladder.

exploration of both the spin and the charge degrees of freedom in the context of Hubbard models defined on two-leg ladder geometries. In fact, computational results for Hubbard ladders with strong rung (or inter-leg) interaction show the presence of a spin gap for all interaction strengths.⁸⁻¹⁰ However, not much is known about the real time dynamics of charge excitations in ladder systems. Given the prospect that highly correlated oxides can become technologically useful for light-to-energy conversion, the understanding of this interplay is very important. A related issue is the role of charge excitations in the transport properties of strongly correlated nanostructures, as highlighted by recent experiments.¹¹

A crucial question is whether charge excitations in a correlated insulator will be able to properly transfer the charge into the metallic contacts, thus establishing a steady-state photocurrent. This has been a motivating factor for studies of exciton-like pairs of charge excitations in Mott insulators¹²⁻¹⁴ and, more recently, in bilayer systems.^{15,16} In Hubbard systems, the elementary charge excitation that preserves the total number of electrons is a “doublon-holon” pair, formed by a double-occupied site (doublon) and an “empty” one (holon), as shown schematically in Fig. 1. In some situations,

the holon and doublon can attract each other forming a ‘‘Hubbard exciton’’, as revealed through spectroscopic evidence by a recent experiment in the transition metal oxide YVO_3 .¹⁷

Thus, it is important to understand how interactions, quantum fluctuations, and dimensionality can affect the lifetime of such charge excitations. In our previous effort,¹² it was shown that the mechanism for holon-doublon decay into magnetic excitations is inefficient in strictly one-dimensional Hubbard chains. In the present paper, we extend these ideas to investigate the dynamics of doublon-holon pairs in Hubbard two-leg ladders, which are qualitatively different from chains due to the presence of a spin gap. We find that the geometry of the ladder strongly affects the propagation of a doublon-holon pair and identify two distinct parameter regimes.

For weak inter-leg coupling, the results are qualitatively similar to the case of the chain^{12,13}, with some renormalization of the parameters. More interestingly is the case of strong inter-leg coupling: in this regime, that is drastically different from a one-dimensional chain, quantities such as the double occupancy and the properties of the excitations (e.g., the doublon speed) are qualitatively affected by the ladder geometry.

The paper is organized as follows: the Hubbard ladder model and the specific technical details of the tDMRG method used are presented in Sec. II and in Appendix A. In Sec. III, we present the results for the charge (Sec. III A) and double occupancy dynamics (Sec. III B) as well as the dependency of the excitation speed with the spin-gap model (Sec. III C). Our concluding remarks are presented in Sec. IV.

II. MODEL AND METHODS

The Hubbard ladder Hamiltonian is written as

$$\hat{H} = \sum_{i,j} t_{ij} \hat{c}_{i\sigma}^\dagger \hat{c}_{i\sigma} + U \sum_i \hat{n}_{i\uparrow} \hat{n}_{i\downarrow}, \quad (1)$$

where the notation is similar to that of Ref. 12. The hopping matrix t , however, now corresponds to that of a two-leg ladder, such that $t_{ij} = t_x$ if i and j are nearest neighbors along the x direction (i.e., the leg direction), $t_{ij} = t_y$ if i and j are nearest neighbors along the y direction, and 0 (zero) otherwise. In the following, we set $t_x = 1$ and use it as our energy unit.

In order to create charge excitations, we define holon- and doublon-creation operators as $h_i^\dagger = \sum_\sigma \hat{c}_{i\sigma} (1 - \hat{n}_{i\bar{\sigma}})$, and $d_i^\dagger = \sum_\sigma \hat{c}_{i\sigma}^\dagger \hat{n}_{i\bar{\sigma}}$ respectively, where $\uparrow = \downarrow$. As in Ref. 12, we model the electron- and hole-like excitations (created by light absorption, for instance) as an excited state $|\Psi_e\rangle = h_i^\dagger d_j^\dagger |\Psi_0\rangle$, where $|\Psi_0\rangle$ is the ground state of the Hubbard-ladder system at half-filling, and i and j are chosen fixed sites where the excitation occurs. For concreteness, as depicted in Figure 1, we choose these sites to be the central sites of the upper leg, which allows

a direct comparison to the results depicted in Refs. 12,13 for the case $t_y = 0$.

Next comes the time evolution of the excited state with the tDMRG method.^{18,19} In order to time-evolve the system, we will use the time-step-targetting Krylov method (Ref. 20 and references therein) and follow the implementation found in Ref. 21. We find this approach to be better suited for generic Hamiltonians in the ladder geometry rather than the Suzuki-Trotter decomposition method, which would require the ladder to be treated as a series of coupled dimers.⁷ We have also compared some results to a Runge-Kutta approach and found excellent agreement.

We calculate the state $|\Psi(\tau)\rangle = e^{-i\hat{H}\tau} |\Psi_e\rangle$, with \hat{H} given by Eq. (1), as a function of time τ (such that $|\Psi(0^+)\rangle = |\Psi_e\rangle$) and then compute real observables as described in Sec. III. Unless otherwise stated, the results shown are for a 20-site (10×2) ladder at half-filling, with time step $\Delta\tau = 0.2$ and times up to $\tau \leq 6$ (in units of \hbar/t_x). As we discuss in Appendix A, accumulated errors during the time evolution introduce a constraint in the accuracy of the results at long time scales. For this reason, we have opted to show results with times only up to $\tau_{\max} = 6$ (see Appendix A for details).

III. RESULTS

In this section, we show results for the local charge and double occupancy at each site, defined respectively as

$$\begin{aligned} \langle n_i \rangle(\tau) &= \sum_{\sigma=\uparrow,\downarrow} \langle \Psi(\tau) | \hat{c}_{i\sigma}^\dagger \hat{c}_{i\sigma} | \Psi(\tau) \rangle / \langle \Psi(\tau) | \Psi(\tau) \rangle, \\ \langle n_i^d \rangle(\tau) &= \langle \Psi(\tau) | \hat{n}_{i\uparrow} \hat{n}_{i\downarrow} | \Psi(\tau) \rangle / \langle \Psi(\tau) | \Psi(\tau) \rangle, \end{aligned} \quad (2)$$

using the state $|\Psi(\tau)\rangle = e^{-iH\tau} |\Psi(0^+)\rangle$. The calculations are performed for a 20-site (10×2) ladder at half-filling unless otherwise noted. In our convention, the sites are labeled as follows: the leftmost upper site is site 0, the leftmost lower site is site 1, and the site index increases by one in the vertical top-down direction and by two in the horizontal-right direction. Thus, even numbered sites (starting at ‘‘0’’) are located in the upper leg and odd-numbered sites are in the lower leg. The doublon-holon pair was created at time $\tau = 0^+$ in the center sites of the upper leg, indicated as sites ‘‘8’’ (holon) and ‘‘10’’ (doublon).

A. Charge dynamics

The typical behavior of the charge $\langle n_i \rangle(\tau)$ as a function of time is shown in Fig. 2 for $U = 10$. Each panel shows the charge configuration of the ladder at a given time τ for $t_y = 0$ (left panels) and $t_y = 3$ (right panels). The top panels show the creation of the doublon ($\langle n \rangle = 2$) and holon ($\langle n \rangle = 0$) excitations in the central sites of the upper leg at $\tau = 0^+$. As time progresses, the

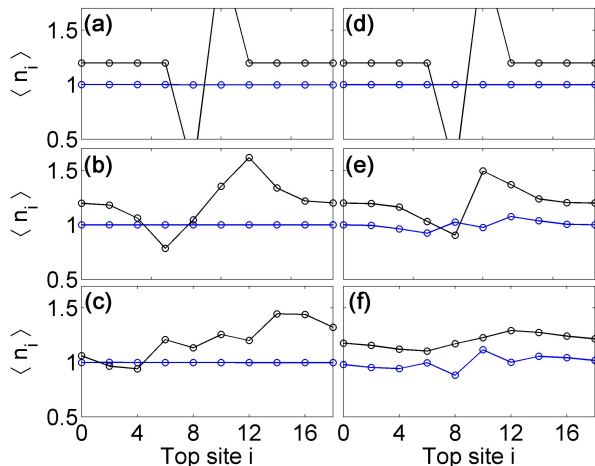


FIG. 2: (Color online) Charge $\langle n_i \rangle$ at each site for different times for the cases $t_y = 0$ (a,b,c) and $t_y = 3$ (d,e,f). Charge values in the upper leg are shifted by 0.2 for better visualization. Times are $\tau = 0$ (panels a,d), $\tau = 1$ (b,e), and $\tau = 2$ (c,f).

excitations propagate throughout the system in opposite directions,¹² eventually reaching the end of the ladder at $\tau \sim 3 - 4$.

More instructive is to show the average charge as a function of time τ on a particular site. Fig. 3 shows $\langle n_i \rangle(\tau)$ at the sites close to the holon-doublon creation point for $U = 10$, $t_x = 1$ and $t_y = 0$ (corresponding to the case of uncoupled ladder legs, with zero spin-gap) and $t_y = 3$ (spin gapped case).

For $t_y = 0$ (left panels in Fig. 3) and $\tau = 0$, the charge at holon and doublon sites is 0 and 2, respectively with $\langle n_i \rangle = 1$ in the remaining sites. As time evolves, the charge on the doublon (holon) site decreases (increases) and oscillates as time progresses. More importantly, the excess (missing) charge is initially transferred to the neighboring sites in the same leg (labeled “6” and “12”) so that the charge excitations “move” throughout the upper leg and, eventually, the local charge on all sites in the upper leg will fluctuate, while keeping the total charge $N = \sum_i \langle n_i \rangle$ constant. As expected, for $t_y = 0$ there is no transfer to the lower leg (Fig 3-b).

For $t_y \neq 0$, the charge excitations will also propagate into the lower leg (Fig. 3-c,d). In the case $t_y = 3t_x$, the dynamics of the local charge on the sites neighboring, say, the doublon site (site “10”) vertically or horizontally will be different, with a large portion of charge oscillating vertically due to the dominance of the hoppings along the y direction ($t_y > t_x$). This can be seen in Fig. 3(c,d) by comparing the charge on sites “11” (first neighbor in the lower leg) and “12” (first neighbor in the upper leg).

We should also point out that, since the time-evolution conserves energy, there is no mechanism for “recombination” of the doublon-holon pair once it is created.¹² Thus, the electron- and hole-like excitations do not “cross” each

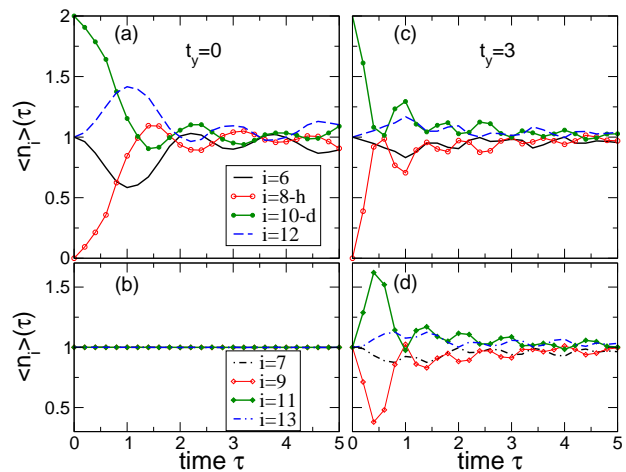


FIG. 3: (Color online) Charge $\langle n_i \rangle$ on sites close to the holon-doublon creation sites (8 and 10) for $t_y = 0$ (a,b), and $t_y = 3$ (c,d).

other, creating a spatial particle-hole asymmetry in the system. This asymmetry is kept throughout the time evolution such that the charge of sites in the “electron side” are related to their “hole side” counterparts by a particle-hole transformation (e.g., $\langle n_{i=12} \rangle(\tau) = 2 - \langle n_{i=6} \rangle(\tau)$).

B. Double Occupancy

The behavior of the double occupancy $\langle n_i^d \rangle \equiv \langle \hat{n}_{i\uparrow} \hat{n}_{i\downarrow} \rangle$ is shown in Figs. 4 and 5. At $\tau = 0^+$, the double occupancy is the maximum ($= 1$) at the doublon site, zero at the holon site and small in the rest of the system (the actual value will depend on U). For $t_y = 0$, the local double occupancy fluctuates as the doublon-holon pair propagates in the upper leg but there is no change in the double occupancy in the lower leg. This is in contrast with the behavior for $t_y > t_x$, for which the propagation of the doublon in the upper leg changes the double occupancy of the sites in the lower leg.

An interesting property seen for $t_y \neq 0$ is that the vertical coupling correlates the double occupancy of sites within the same “rung”. This is clearly shown in Fig. 4-d, which shows the double occupancy at $\tau = 0^+$ (compare it with the $t_y = 0$ case Fig. 4-a): the creation of a holon or a doublon on a given site also changes the double occupancy in the site directly below it. This happens even in the non-interacting case and it is a natural consequence of the dominance of the rungs in the $t_y \gg t_x$ regime.

This effect can be better visualized by looking at the double occupancy for individual sites as a function of time (Fig. 5). For $t_y = 3$ (Fig. 5-c,d) and time $\tau = 0^+$, when the holon-doublon pair is created at sites 8 and 10, the double occupancy at sites in the same rungs (9 and 11, respectively) is reduced to zero. This is in contrast with the other sites in the lower leg (say, sites 7 and 13), which retain the ground-state double occupancy value.

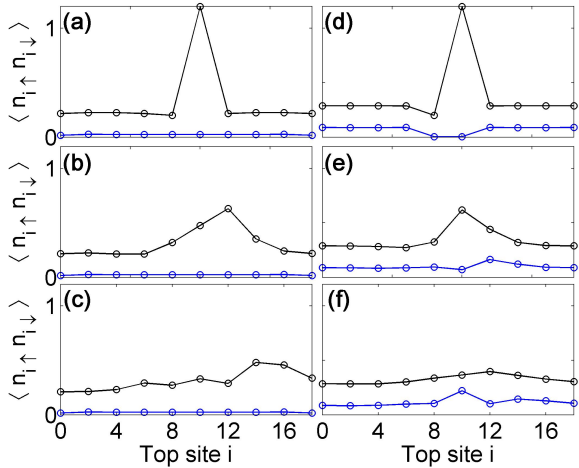


FIG. 4: (Color online) Double occupancy $\langle n_{i\uparrow} n_{i\downarrow} \rangle$ at each site for different times for the cases $t_y = 0$ (a,b,c) and $t_y = 3$ (d,e,f). Double occupancy values in the upper leg are shifted by 0.2 for better visualization. Times are $\tau = 0$ (a,d), 1 (b,e), and 2 (c,f).

This is quite different from the case of uncoupled legs ($t_y = 0$, Fig. 5-a,b), for which no change in the double occupancy happens in the lower leg, as expected.

This “non-local” change in the double occupancy in the lower leg when a doublon is created in the upper leg can be illustrated in a very simple model. Let us consider a single, two-site rung (say, sites 0 and 1) with a hopping term $H_{\text{rung}} = t_y \sum_{\sigma} \hat{c}_{0\sigma}^{\dagger} \hat{c}_{1\sigma} + \text{h.c.}$ between them. The ground state $|\text{GS}\rangle$ of H_{rung} lies in the two-electron sector (with energy $-2t_y$) and it is given by

$$|\text{GS}\rangle = \frac{1}{2} \left(-\sqrt{2} |S\rangle_{\text{rung}} + |D_0\rangle + |D_1\rangle \right), \quad (3)$$

where $|S\rangle_{\text{rung}} = (1/\sqrt{2}) (|\uparrow\rangle_0 |\downarrow\rangle_1 - |\downarrow\rangle_0 |\uparrow\rangle_1)$ is a rung spin singlet involving spins on sites 0 and 1 and $|D_{0(1)}\rangle = |\uparrow\downarrow\rangle_{0(1)} |0\rangle_{1(0)}$ are doubly occupied states.²²

Notice that the double occupancy is the *same* in both sites: $\langle \text{GS} | \hat{n}_{0(1)\uparrow} \hat{n}_{0(1)\downarrow} | \text{GS} \rangle = 1/4$. Now, if a doublon is created at site 0, then the (normalized) state becomes:

$$|\psi_{d0}\rangle = d_0^{\dagger} |\text{GS}\rangle = |\uparrow\downarrow\rangle_0 \otimes \frac{(|\uparrow\rangle_1 + |\downarrow\rangle_1)}{\sqrt{2}}, \quad (4)$$

and, obviously, the double occupation in site 0 is now equal to 1. Notice, however that the double occupancy in site 1 will be *reduced*, since $\langle \psi_{d0} | \hat{n}_{1\uparrow} \hat{n}_{1\downarrow} | \psi_{d0} \rangle = 0$, hence a “non-local” change in double occupancy occur at site 1 as the doublon is created in site 0.

Another interesting feature of the large t_y regime is the “beating” of both charge and double occupancy within the rung where the doublon is created. Figs. 3-(c,d) and 5-(c,d) show that, as time evolves, the charge and double occupancy in site 11 oscillate with the same period but out of phase with their counterparts in site 10. Interestingly, for the “holon rung” (sites 8 and 9) these beatings

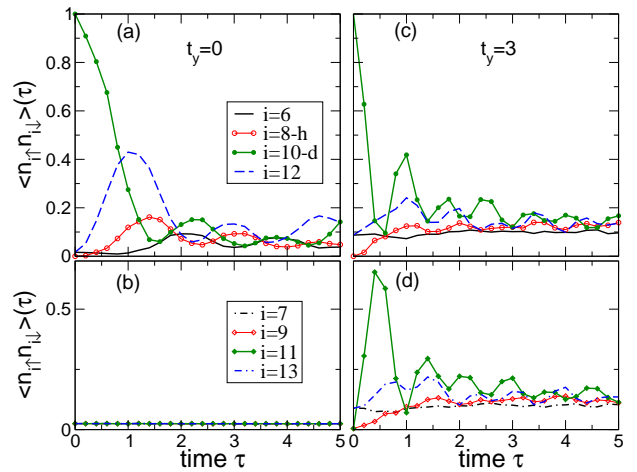


FIG. 5: (Color online) Double occupancy versus time at sites close to the holon-doublon creation sites (8 and 10) for $t_y = 0$ (a,b) and $t_y = 3$ (c,d).

show up only in the charge (Fig. 3-c,d) but not in the double occupancy (Fig. 5-c,d).

Next, we look at the total double occupancy $N_d(\tau) = \sum_i \langle n_i^d \rangle(\tau)$. In contrast with the total charge (which is conserved and therefore independent of τ), $N_d(\tau)$ fluctuates with time τ for $U \neq 0$. As in Ref. 12, we look at the quantity $\Delta N_d(\tau) = N_d(\tau) - N_d^{(0)}$ where $N_d^{(0)} = \langle \Psi_0 | n_i^d | \Psi_0 \rangle$ is the total ground-state double occupancy. This “excess double occupancy” is shown in Fig. 6.

We note that the value of $\Delta N_d(0)$ will depend on t_y . For $t_y = 0$, the creation of the holon-doublon pair only changes the double occupancy locally and therefore $\Delta N_d(0) = 1 - (\langle \Psi_0 | n_{ih}^d | \Psi_0 \rangle + \langle \Psi_0 | n_{id}^d | \Psi_0 \rangle)$ where ih and id label the sites where the holon and doublon are created, respectively. By contrast, for $t_y \neq 0$, the creation of a doublon-holon pair will change the double occupancy on the other sites of the rungs as well (as discussed above) by an amount that increases with t_y . Thus, $\Delta N_d(0)$ decreases with t_y , as shown in the inset in Fig. 6. The decrease is much accentuated for $t_y \geq 2$, establishing a clear qualitative distinction from the results for the one-dimensional case $t_y = 0$, where $\Delta N_d(0)$ is “local” in the sense that it depends only on the ground-state double occupancy at the sites where the holon-doublon is created.¹²

For longer times, $\Delta N_d(\tau)$ reaches a plateau with a height that also decreases with t_y . For $U = 10$ and large t_y , $\Delta N_d(\tau)$ fluctuates around a value that is essentially independent of τ , with no sizeable decay in double occupancy with time. This is shown in the inset of Fig. 6 where $\Delta N_d(\tau = 0^+)$ and $\Delta N_d(\tau = 6)$ are plotted as a function of t_y . For $t_y = 0$ and different values of U , the value of $\langle \Delta N_d \rangle_{\tau}$ increases with U , consistently with the findings of Ref. 12.

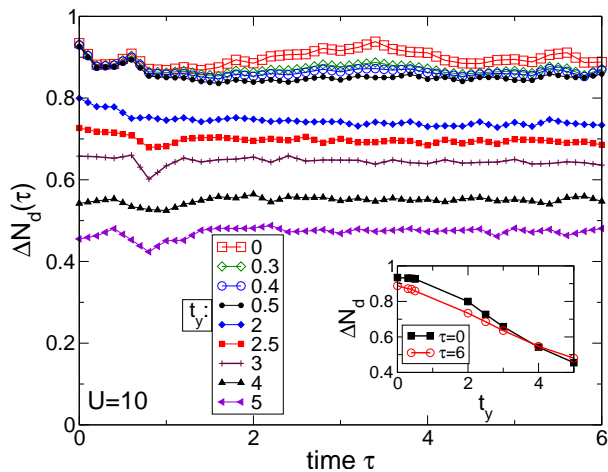


FIG. 6: (Color online) Excess double occupancy $\Delta N_d(\tau)$ versus τ for $U = 10$ and different values of t_y . Inset: ΔN_d at fixed times ($\tau = 0$ and $\tau = 6$) versus t_y .

C. Doublon speed

A clear difference in behavior between the two regimes (small and large t_y) can be captured by the speed at which the charge excitations travel, particularly the doublon. This is illustrated in Fig. 7 which shows the double occupancy vs time at site “18”, located in the upper leg and at the right end of the ladder.

The position of the first peak in $\langle n_{di} \rangle(\tau)$ marks the “arrival time” τ_a of the doublon and can be used to infer its “speed” $v_d \propto \tau_a^{-1}$. In Fig. 7, we can identify two distinct regimes: for $t_y \leq 1$ (Fig. 7-a), such arrival times are of order $\tau_a \sim 3$ while for $t_y > 1$ (Fig. 7-b), arrival times are substantially higher, in the $3 < \tau_a \lesssim 4$ range. Thus, the doublon effectively moves “faster” (smaller arrival times) for small values of the inter-leg coupling t_y .

The clear difference in arrival times in the two regimes is striking. Some hints as to why it comes about can be found in the curve for $t_y/t_x \sim 1$. In the transition between the two regimes ($t_y/t_x \sim 1$), a second peak, with a longer arrival time, becomes more prominent than the first peak. As t_y increases, this second peak dominates and effectively marks the arrival of the doublon. In fact, this second peak arises as a result of the part of the doublon that travels through the *lower leg* instead of the upper one for large t_y , as shown in Figs. 4 and 5.

A curious behavior is that, within both regimes ($t_y \leq 0.5$ and $t_y \geq 2$), the horizontal doublon speed increases with the coupling between the ladder legs. This is shown in the inset, where τ_a^{-1} is plotted as a function of t_y (circles). We notice that, within each regime, τ_a^{-1} (taken from the more prominent peak at each regime, except for $t_y = 1$ where two values are used) does not depend linearly with t_y , indicating that such increase does not arise from a simple rescaling of the “time unit” in terms of \hbar/t_y .

In addition, the scaling of τ_a^{-1} with t_y is different in

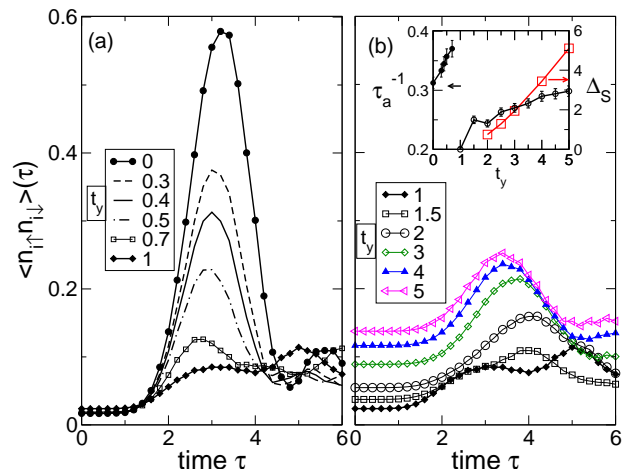


FIG. 7: (Color online) Double occupancy at a site at the end of the ladder for (a) $t_y \leq 1$ and (b) $t_y \geq 1$ (no shift added). The position of the peak marks the “arrival time” τ_a of the doublon. Inset: inverse doublon arrival time τ_a^{-1} (circles) and spin-gap calculated for a 2×32 ladder (squares) vs t_y . Error bars are given by $\Delta\tau/\tau^2$ and indicate the uncertainty in the determination of the arrival time given the time step $\Delta\tau$.

each regime and therefore one might speculate if there is an extra energy scale dominating the behavior of τ_a^{-1} at large t_y . As it is known from previous studies,⁹ Hubbard two-leg ladders display a sizeable spin gap in the large t_y regime. One possibility would be that the propagation of the doublon would be coupled to $S = 1$ spin excitations (where a singlet in a rung becomes a triplet), thus resulting in a scaling of the doublon speed with the spin gap.

In order to check for such a connection between τ_a^{-1} and the spin gap Δ_s , we have calculated Δ_s for $t_y/t_x \geq 2$. The spin gap can be calculated with DMRG as

$$\Delta_s = E(N/2 + 1, N/2 - 1) - E(N/2, N/2) \quad (5)$$

where $E(N_\uparrow, N_\downarrow)$ is the energy of a state with N_\uparrow electrons with spin up and N_\downarrow electrons with spin down (total $N = N_\uparrow + N_\downarrow$ electrons). We have performed these (static) calculations for a 2×32 ($N = 64$) ladder with $U = 10$ at half-filling.

The results are shown in the inset of Fig. 7. Although the results do not show a clear scaling of the type “ $\tau_a^{-1} \propto \Delta_s$ ”, the dependence of τ_a^{-1} with t_y is markedly different in the strong spin-gap regime as compared to “small t_y ” one: the rate of increase of the doublon speed is lower for $t_y > 2t_x$, where a clear spin gap is present. This indicates that the propagation of the doublon might be coupled to magnon-like spin excitations, although this connection is weak. This is also consistent with the rather weak decay shown in Fig. 6 even in the large t_y regime.

IV. CONCLUSIONS

In this work, we have investigated the dynamics of holon-doublon pairs in Hubbard two-leg ladders using the time-dependent DMRG method. The geometry of the ladder brings some interesting qualitative changes as compared to the case of the chains. A telling example is a “non-local” character of the double occupancy: the creation of a doublon in a site at the upper leg *reduces* the double occupancy in the bottom site coupled to it. This, in fact, reduces the total double occupancy as the inter-leg coupling increases.

In addition, we have found important qualitative differences in the dynamics of the excitations depending on the relative coupling between the ladder legs. For weak inter-leg coupling ($t_y/t_x \ll 1$), results are qualitatively similar to the strictly one-dimensional case.^{12,13} However, the results show a strong downward shift in the doublon horizontal speed as one crosses over from weak ($t_y/t_x \ll 1$) to strong ($t_y/t_x \gg 1$) inter-leg coupling. We attribute this shift to different propagation “paths” for the doublon: for small t_y , the doublon propagates mainly through the sites of a single leg. For large t_y , the propagation involves also the vertical direction (through the ladder rungs rather than single sites), effectively “slowing down” the doublon.

An intuitive physical picture of the doublon propagation in the $t_y \gg t_x$ regime emerges by noticing that, in this regime, it is often a good approximation^{4,5} to assume that the ground state of the ladder system is made out of individual rung states, such as the one given by Eq. 3. For strongly interacting ladders, the rung ground state has a strong contribution from the spin singlet $|S\rangle_{\text{rung}}$.²² Thus, the excitations propagate in a “background” of spins tightly packed into singlets. The propagation then “damages the background”, causing a reduction of the excitation’s speed. We note that this is in sharp contrast with the one-dimensional case, where no “spin-singlet background” is present.

Moreover, although in both regimes ($t_y/t_x \ll 1$ and $t_y/t_x \gg 1$) the “horizontal” speed of the doublon increases as the vertical coupling increases, the scaling of the doublon speed with t_y is different, being less pronounced in the strong inter-leg coupling regime. Our results indicate that the presence of a spin gap qualitatively changes such scaling, indicating a possible (although weak) coupling between the doublon and spin excitations.

Acknowledgments

We thank Khaled Al-Hassanieh and Adrian Feiguin for fruitful discussions. This work was supported by the Center for Nanophase Materials Sciences, sponsored by the Scientific User Facilities Division, Basic Energy Sciences, U.S. Department of Energy, under contract with UT-Battelle. This research used resources of the

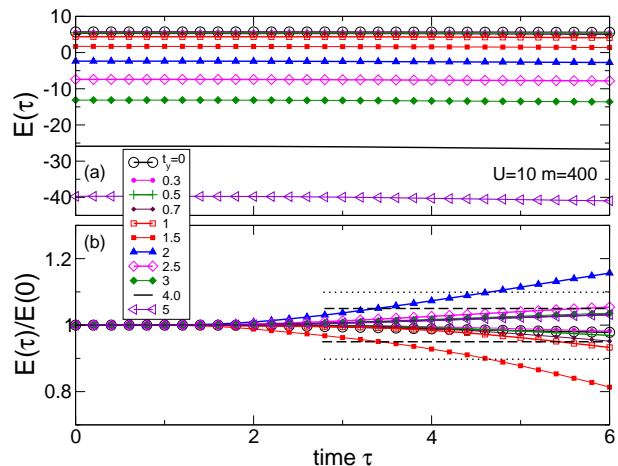


FIG. 8: (Color online) (a) Average energy $E(\tau)$ as a function of τ for $U = 10$ with $m = 400$ kept states and different values of t_y . In (b), $E(\tau)/E(0)$ is plotted, with dashed and dotted horizontal lines marking the 5% and 10% “confidence ranges” respectively.

National Center for Computational Sciences, as well as the OIC at Oak Ridge National Laboratory. L.D.S acknowledges support from Brazilian agencies CNPq and FAPESP (Grant No. 2010/20804-9). G.A. acknowledges support from the DOE early career research program. E.D. is supported in part by the U.S. Department of Energy, Office of Basic Energy Sciences, Materials Science and Engineering Division.

Appendix A: Accuracy during time evolution

In this section, we discuss some technical aspects regarding the accuracy of the results. In addition to the usual criteria for detecting loss of accuracy during time evolution (namely, an exponential increase of the truncation error for a given number m of kept states, leading to a “runaway time”²³), we have also monitored the energy expectation value $E(\tau) \equiv \langle \Psi(\tau) | \hat{H} | \Psi(\tau) \rangle / \langle \Psi(\tau) | \Psi(\tau) \rangle$ with increasing τ as a way to probe the accuracy of the results for longer time scales. Since the Hamiltonian in Eq. 1 is time-independent, the expectation is that this quantity should be constant (i.e., $E(\tau) = E(0)$) and thus deviations from $E(\tau) = E(0)$ can be used as a gauge of the accumulation of numerical errors during the time evolution of the system.

The results for $E(\tau)$ are shown in Fig. 8. As time progresses, the accumulated errors during the time evolution cause $E(\tau)$ to deviate from the value at $\tau = 0$. Since we have opted to keep U and t_x fixed (no rescaling), the numerical value of $E(0)$ (the average energy of the system after the creation of the holon-doublon pair) will change significantly as t_y is increased (Fig. 8-a). For better visualization, we have also plotted $E(\tau)/E(0)$ (Fig. 8-b), which gives a measure of the relative “degradation” (i.e.,

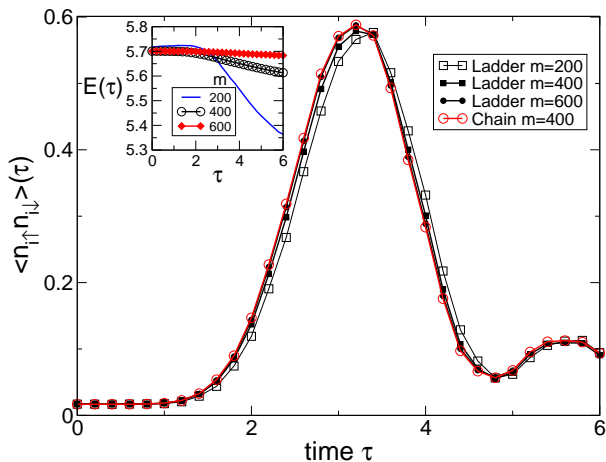


FIG. 9: (Color online) Comparison between ladder and chain calculations: double occupancy at a site located near the end of the system vs time for a chain with $m = 400$ kept states and a ladder with $t_y = 0$ and $m = 200, 400$ (same data as in Fig. 7-a) and 600 kept states. Inset: $E(\tau)$ in the ladder for $t_y = 0$ and different number of kept states during the time evolution.

the deviation from $E(\tau)/E(0) = 1$). As seen in Fig. 8-b, this “degradation” in energy will increase with time but it is within 5% accuracy up $\tau \sim 6$, using $m = 400$ states during the time evolution and time step $\Delta\tau = 0.2$, which we consider acceptable.

We should note that, as can be inferred from Fig. 8-a, $E(0)$ passes through zero and becomes negative for $t_y \sim 1.75$, causing $E(\tau)/E(0)$ to be larger than 1 for $t_y \gtrsim 1.75$ although $E(\tau) < E(0)$ in general (i.e., the

average energy always *decreases*). Additionally, the fact that $E(0)$ is relatively small ($|E(0)| < 5$) for t_y in the range $1.5 - 2$ makes the deviation from $E(\tau)/E(0) = 1$ to be larger (see Fig. 8-b), although this does not imply a larger accumulated error (in fact, in this t_y range, $|E(\tau) - E(0)| < 0.4$ up to $\tau \sim 6$).

Another important accuracy test is a comparison between the propagation of the holon-doublon in an uncoupled ladder ($t_y = 0$) and in a one-dimensional chain. These should yield similar results if the number of kept states m is sufficiently large. As shown in Fig. 9, we find that using $m = 400$ kept states in the ladder reproduces the chain results for the double occupancy quite well at a quantitative level up to $\tau \sim 6$. In fact, even a much smaller number of kept states $m = 200$ already give the correct qualitative behavior. Moreover, we find that increasing m above $m = 400$ does not modify the trends and/or numerical values appreciably: the results for the time-dependence of observables such as double occupancy are essentially unchanged up to $\tau \sim 6$.

Thus, the results presented in the paper (e.g., the doublon speed in Fig. 7) calculated with $m = 400$ will not be significantly modified by increasing m . Keeping more states (say, $m = 600$) during time evolution brings only a slight improvement in both the observables and also in $E(\tau)$. This latter point is illustrated in the inset of Fig. 9, where $E(\tau)$ is shown for $t_y = 0$ and different values of m . For this reason, the calculations presented in this paper were performed keeping up to $m = 400$ states during the time evolution, as increasing the number of retained states to $m = 600$ does not justify the considerable extra computational cost.

¹ E. Dagotto, Rep. Prog. Phys. **62**, 1525 (1999).

² E. Dagotto, J. Riera, and D. Scalapino, Phys. Rev. B **45**, 5744 (1992).

³ S. R. White, R. M. Noack, and D. J. Scalapino, Phys. Rev. Lett. **73**, 886 (1994).

⁴ G. B. Martins, M. Laukamp, J. Riera, and E. Dagotto, Phys. Rev. Lett. **78**, 3563 (1997).

⁵ M. Laukamp, G. B. Martins, C. Gazza, A. L. Malvezzi, E. Dagotto, P. M. Hansen, A. C. López, and J. Riera, Phys. Rev. B **57**, 10755 (1998).

⁶ T. M. Rice, S. Gopalan, and M. Sigrist, EPL **23**, 445 (1993).

⁷ P. Bouillot, C. Kollath, A. M. Läuchli, M. Zvonarev, B. Thielemann, C. Rüegg, E. Orignac, R. Citro, M. Klanjšek, C. Berthier, et al., Phys. Rev. B **83**, 054407 (2011).

⁸ R. M. Noack, S. R. White, and D. J. Scalapino, EPL **30**, 163 (1995).

⁹ R. Noack, S. White, and D. Scalapino, Physica C **270**, 281 (1996).

¹⁰ R. M. Noack, N. Bulut, D. J. Scalapino, and M. G. Zacher, Phys. Rev. B **56**, 7162 (1997).

¹¹ J. Wei and D. Natelson, Nanoscale **3**, 3509 (2011).

¹² K. A. Al-Hassanieh, F. A. Reboredo, A. E. Feiguin, I. González, and E. Dagotto, Phys. Rev. Lett. **100**, 166403 (2008).

¹³ L. G. G. V. Dias da Silva, K. A. Al-Hassanieh, A. E. Feiguin, F. A. Reboredo, and E. Dagotto, Phys. Rev. B **81**, 125113 (2010).

¹⁴ R. Sensarma, D. Pekker, M. D. Lukin, and E. Demler, Phys. Rev. Lett. **103**, 035303 (2009).

¹⁵ L. Rademaker, K. Wu, H. Hilgenkamp, and J. Zaanen, EPL **97**, 27004 (2012).

¹⁶ L. Rademaker, K. Wu, and J. Zaanen, New Journal of Physics **14**, 083040 (2012).

¹⁷ F. Novelli, D. Fausti, J. Reul, F. Cilento, P. H. M. van Loosdrecht, A. A. Nugroho, T. T. M. Palstra, M. Gruninger, and F. Parmigiani, arXiv:1205.4609 (2012).

¹⁸ S. R. White and A. E. Feiguin, Phys. Rev. Lett. **93**, 076401 (2004).

¹⁹ A. J. Daley, C. Kollath, U. Schollwöck, and G. Vidal, J. Stat. Mech.: Theory Exp. **2004**, P04005 (2004).

²⁰ S. R. Manmana, A. Muramatsu, and R. M. Noack, in *AIP Conf. Proc.* (2005), also in <http://arxiv.org/abs/cond-mat/0502396v1>.

²¹ G. Alvarez, L. G. G. V. Dias da Silva, E. Ponce, and

E. Dagotto, Phys. Rev. E **84**, 056706 (2011).

²² In the interacting case, the contributions of $|D_1\rangle$ and $|D_2\rangle$ to $|\text{GS}\rangle$ in Eq. 3 will decrease as $\sim t_y/U$ and $|S\rangle_{\text{rung}}$ becomes the rung ground state in the $U/t_y \rightarrow \infty$ limit, akin

to the case of spin ladders.^{4,5}

²³ D. Gobert, C. Kollath, U. Schollwöck, and G. Schütz, Phys. Rev. E **71**, 036102 (2005).